

The formation of desilication products in the presence of kaolinite and halloysite – the role of surface area

Jose F. Gomes¹, Michael Davies², Peter Smith², Franca Jones^{1*}

1. School of Molecular and Life Sciences, Chemistry, Curtin University, GPO Box U1987, Perth WA 6845

2. CSIRO Mineral Resources, PO Box 7229, Karawara, WA 6152, Australia

Abstract

A great deal of effort has been dedicated to improve the fundamental understanding of the mechanism of desilication product crystallization under Bayer process refinery conditions. Differences in the mineralogy of the reactive silica found in bauxite could change the kinetics and possibly the formation pathways of the desilication product formation. In this work, halloysite was investigated and compared to kaolinite, which is commonly found in bauxite. Different ratios of kaolinite and halloysite were used to form desilication product and the solids formed were characterized thoroughly to determine the impact the presence of the clay had. In addition, differences in dissolution rate due to the presence of halloysite was determined. The results show that the presence of halloysite led to a faster dissolution rate of the clay overall, which can be attributed to the total specific surface area of the reactive silica source. Thus, the crystallinity of the clay was found to have limited impact. The presence of halloysite also increased the *measured* maximum solution [SiO₂] in the liquor, which in turn increases the driving force for the formation of desilication product. The increase in halloysite content thus results in desilication product being observed at an earlier stage and, overall, leads to an enhanced rate of desilication product formation.

1. Introduction

In the Bayer process, alumina-containing minerals present in the bauxite ore are dissolved in a hot caustic solution, separated from non-soluble impurities and re-precipitated in the form of gibbsite (Al(OH)₃). The gibbsite can then be calcined to produce alumina. The conditions used in the process depends on the mineralogy of the bauxite and the impurities introduced with the ore, for example boehmite versus gibbsite in the ore and the silica content from clays and quartz.

Bauxite is a weathered product derived from natural aluminous rocks. Significant chemical and mineralogical variations caused by different parent rocks and weathering can be observed in the bauxite deposits as evidenced by the type and amount of extractable aluminum (oxy-)hydroxides (e.g. gibbsite and boehmite), iron oxides, the silica-containing minerals (clay minerals and quartz) and the crystallinity and particle size of these compounds. Reactive silica (R_xSiO₂) is the common term used by the alumina industry to describe the silica that dissolves ~~in the liquor~~ under process conditions. The strict control of the desilication reactions, especially residual levels of silica in solution, is important to avoid downstream issues such as silica scaling (especially in heat exchangers) and silica impurity levels in product gibbsite.

The clay minerals present in lateritic bauxites (~90% of world's bauxite reserves) (Fressinet et al., 2005) and karstic bauxites can include kaolinite, halloysite, dickite,

muscovite and illite (Gan et al., 2013), all of which have the potential to react with the hot caustic and re-precipitate to forming sodium aluminosilicates, collectively known as desilication products (DSPs). Generally, kaolinite is the major source of reactive silica in the Bayer process (Smith 2009). Due to this, most literature investigates the kinetics, the formation and the transformation of DSPs under Bayer conditions with kaolin/kaolinite (Cardile et al., 1994; Jones and Smith, 2008; LaMacchia, 2012; Laws, 2005). Since the major form of silica (quartz) in bauxite is unreactive under low temperature conditions it is assumed that between 70% to 80% of the total *reactive* silica ($RxSiO_2$) present in the bauxite of Western Australian mines is due to kaolinite. In Darling Range bauxite (Western Australia), kaolinite and halloysite are common clay minerals responsible for the reactive silica content in the Bayer process (Anand et al., 1991), and halloysite is also known to occur in other younger bauxite deposits (Hose, 2013) but is difficult to differentiate from kaolinite unless halloysite is in its tubular form and is observed through microscopy. Thus, it is unclear how much halloysite is found in Darling Range or other bauxite ores, but the work of Anand and Hose clearly indicate that it should be present (Anand et al., 1991; Hose, 2013).

Kaolinite ($Al_2Si_2O_5(OH)_4$) and halloysite ($Al_2Si_2O_5(OH)_4 \cdot nH_2O$) are both 1:1 phyllosilicates (1 tetrahedral SiO_4 :1 octahedral AlO_6 sheet) linked by oxygen bonding. These two clays have similar chemical composition but differ in their physical structure, water content, specific surface area (SSA) and reactivity. Thus, halloysite has a similar composition to kaolinite but has additional interstitial water (with $n=2$ usually) and the d-spacing of the d_{001} basal plane is 10 Å compared to 7 Å for kaolinite. Halloysite usually has a hollow, cylindrical morphology composed of internal and edge surfaces terminated by Al–OH and Si–OH with external hydrophobic siloxane (Si–O–Si) groups (Figure 1, Tan et al., 2016). The similarities in chemistry and bonding structure makes the differentiation and quantification of kaolinite and halloysite in the bauxite XRD a difficult task. For these reasons, it is unclear how much halloysite is in Darling Range bauxites.

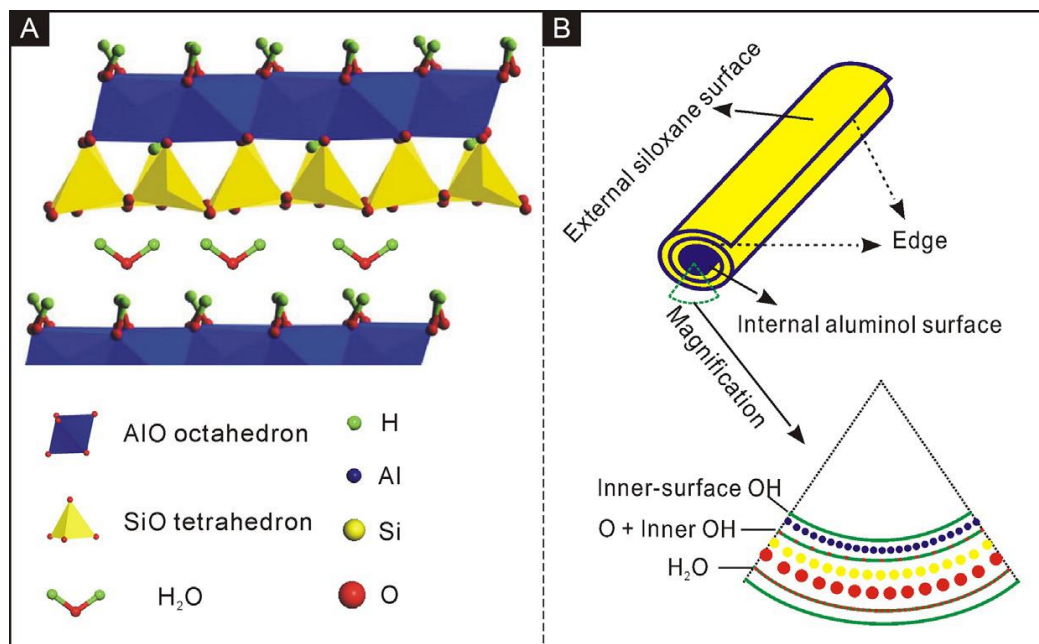


Figure 1: Schematic showing cylindrical morphology of halloysite tubes (with permission of Yuan et al., 2015)

It has been suggested (Radomirovic et al., 2013, Smith et al., 2002, Barnes, 1999) that the reaction of the R_xSiO_2 between the clay minerals and the Bayer liquor *could follow the transformation mechanism* to a more stable DSP phase *via* the pathway shown in Figure 2. An amorphous phase has been observed for solution silicate (Radomirovic et al., 2013) while the LTA phases was observed by Smith et al., 2002 in a synthetic liquor using metasilicate (Na_2SiO_3) as the silicate source. Normally, sodalite [$Na_6(Al_6Si_6O_{24}).mNa_2X.yH_2O$] is the observed product at pre-desilication conditions (Smith, et al., 2001) with **X** (SO_4^{2-} , OH^- or CO_3^{2-}) being the major ions included in the cage. Cancrinite is the more thermodynamically stable form compared to sodalite and is observed when higher digestion temperatures and/or longer formation times are used. However for cancrinite, which has a similar stoichiometry but different crystal structure, X is predominantly CO_3^{2-} . Thus, kinetics plays an important role in these systems.



Figure 2: Possible transformation mechanism pathway of aluminosilicates to the most stable phase.

The structure of sodalite (SOD) is cubic with space-group P43n or P23, depending on the impurities in the liquor (Vogrin et al., 2018). The negative framework charge (3-) is compensated by three sodium cations and at full occupancy of the β -cages, a monovalent anion is included in each cage or a divalent anion in every other cage (Smith et al., 2008). The formation of SOD has the positive effect of reducing the liquor [SiO_2] and encapsulating other impurities that are harmful to the Bayer process, however, it also removes a portion of sodium and aluminum from the liquor thereby increasing production costs.

According to Roach and White (1988), differences in the bauxite mineralogy, especially the R_xSiO_2 components, results in different dissolution rates. They observed that the R_xSiO_2 in a sample containing both kaolinite and halloysite dissolved 1.4 times faster in synthetic liquor compared to kaolinite only. Using a bauxite sample (Darling Range) containing more halloysite than the kaolin/halloysite sample, the dissolution kinetics was up to two times faster. The authors concluded that the differences in the dissolution rate was related to (i) the lower crystallinity of halloysite compared to kaolinite, (ii) the particle size differences and (iii) the increased SSA of halloysite. Importantly, Roach and White (1988) were unable to quantify the amount of halloysite in the samples. Thus, this work was qualitative but poses an important question about whether the halloysite impacts only through surface area effects (Bauer et al., 1998) or whether it behaves differently to kaolinite. In fact, halloysite has extra reaction sites available through the exposed hydroxyl groups (Al-OH and Si-OH), which could affect the dissolution rate and increase the rate of precipitation of DSP. This in turn may improve liquor desilication by achieving either faster desilication rates or lower equilibrium solution silicate concentrations. The kinetic rate of aluminosilicate dissolution was investigated by Carroll-Webb & Walther (1988) who suggested that the reaction of kaolinite was chemically controlled by the surface charge at highly alkaline pH ($pH \geq 11$). A recent review (Schott et al., 2009) showed that the rates of mineral dissolution are controlled by activated complexes formed with exposed hydroxyl groups at the mineral surfaces.

In this study, well-characterized kaolinite and halloysite clays were used and compared. The impact of SSA, the differences between kaolinite and halloysite dissolution and the transformation to DSPs at low temperature (90 °C) were investigated. In addition, whether the clays did or did not proceed by the hypothesized mechanism in Figure 2 was investigated. Such a study will broaden our knowledge of these two clays in the Bayer Process and how they impact the overall desilication kinetics and DSP formation rate. The mineralogical variations introduced into the Bayer process through different bauxite ores need to be determined so that the kinetics of clay dissolution and the mechanisms surrounding the formation of DSPs can be completely understood.

2. Experimental

A set of leaching experiments were conducted in synthetic Bayer liquor at low and high RxSiO_2 concentrations. These conditions were specifically designed to observe the effect of increased SSA on the dissolution rate of RxSiO_2 and the formation of DSP. This included varying the ratios of halloysite at conditions commonly found in the refineries. The percent solids by weight of kaolinite and halloysite in each experimental case are shown in Table 1, where the control is 100% kaolinite (pure kaolinite) and this establishes the basis with which to compare our results and analyze the effects of increasing the initial SSA on desilication. In each case where halloysite was added, it was done so at a constant solids concentration by weight; 11.00 gL^{-1} (low silicate levels) or 22.00 gL^{-1} (high silicate levels). The RxSiO_2 concentration equivalent in solution was then calculated, based on their chemical formula and mass added, resulting in RxSiO_2 values of $5.00 \pm 0.50 \text{ gL}^{-1}$ (low) and $10.00 \pm 1.00 \text{ gL}^{-1}$ (high).

Table 1: Experimental cases used to analyze the impacts of SSA on the kinetics of DSP formation.

Silicate Source	Control	Case 1	Case 2	Case 3	Case 4
Kaolinite %	100	70	50	30	0
Halloysite %	0	30	50	70	100
Total SSA (m^2)	340.8	574.9	731.0	887.0	1121.1

~~The clay samples were added at constant RxSiO_2 but with different kaolinite to halloysite ratios to the reactor vessel with Bayer synthetic liquor.~~

2.1. Liquor preparation and analysis

To prepare synthetic Bayer liquor (1.0 L) analytical grade (Sigma-Aldrich) sodium hydroxide pellets (NaOH), sodium carbonate (Na_2CO_3) and sodium sulphate (Na_2SO_4) were used, by initially dissolving the sodium hydroxide in DI water (400 ml) and subsequently mixing in gibbsite powder (C33, Alcoa Arkansas). The slurry was then heated for approximately 40 minutes to ensure that all the solids were dissolved. A solution of the sodium salts was made separately such that the final concentrations was achieved ($\text{Na}_2\text{CO}_3 = 20 \text{ gL}^{-1}$ and $\text{Na}_2\text{SO}_4 = 15 \text{ gL}^{-1}$) by dissolving the powders in DI water (100 ml) and adding this solution to the initial concentrated sodium aluminate solution. The final solution was filtered using $0.45 \mu\text{m}$ caustic resistant membrane in a

pressure filter. The cooled, filtered synthetic Bayer liquor was then diluted with DI water to the final volume of 1.0 L.

The synthetic liquor was analyzed by automated titration, using Metrohm hardware and software using Connop's method (Connop, 1996) to ensure the concentrations of alumina (A, in terms of Al_2O_3) 60 gL^{-1} , total caustic (C, equivalent Na_2CO_3) 200 gL^{-1} , A/C 0.31 and C/S 0.95 (where S is total soda in gL^{-1}) in the synthetic liquor were within an acceptable required range equivalent to a spent liquor. The terms A, C and S are standard industry nomenclature (Radomirovic et al., 2013). Table 2 gives the average liquor concentration used for all experiments.

Table 2: The Bayer synthetic liquor composition used in all experiments.

A (gL^{-1})	C (gL^{-1})	S (gL^{-1})	A/C	C/S
62.29	203.58	220.57	0.31	0.92
± 0.5	± 1.55	± 1.45	± 0.00	± 0.01

In addition, the liquor contained impurity concentrations typically found in the Bayer process refinery ($\text{Na}_2\text{CO}_3 = 20.0 \text{ gL}^{-1}$ and $\text{Na}_2\text{SO}_4 = 15.0 \text{ gL}^{-1}$)

2.2. Clay characterization

Two different solid silicates, kaolinite (English China clay – Eckalite Kaolin) and halloysite (Sigma-Aldrich – Nanoclay) were used as the sources of reactive silica. The X-ray diffraction (XRD) patterns and scanning electron microscopy (SEM) images used instruments at the John de Laeter Centre at Curtin University. The presence of halloysite in the kaolinite used was considered negligible as it could not be identified by XRD or SEM.

The initial clay materials and the DSPs formed were characterized by XRD using a Bruker D8 Advance instrument. The instrument uses a LynxEye detector, Cu $K\alpha$ irradiation source at 40 kV, the 2θ range was from 5 to 60° with a step size of 0.015° 2θ and a scan speed of 0.5s per step size. The peak position for the different silicate sources and DSP phases present were identified using DIFFRAC.EVA 3.2 (Bruker) software and compared to the Powder Diffraction file (PDF4+ 2018 edition). In addition, qualitative information on the amount of clay and DSP formed was determined through fitting of the patterns obtained from the solids collected in the high R_xSiO_2 experiments in TOPAS (DIFFRAC.TOPAS Bruker version 5). For the 100% kaolinite case the DSP formed was sodalite and Rietveld fitting was performed. For the 100% halloysite case the broadness of peaks for the clay meant Rietveld fitting was not ideal and the direct derivation method of Toraya (2018) was also undertaken. Due to the similarity of the peaks present for kaolinite and halloysite, the mixtures of the clays could not be analysed in this way. See *Supporting Information A1*.

2.2.1. Scanning Electron Microscopy:

The morphology of the DSP formed at different times as well as the initial kaolinite and halloysite clays were examined using SEM. Images were collected in a high-resolution ZEISS NEON 40EsB – FESEM. Solids were prepared on carbon coated stubs and then sputtered with Pd.

2.2.2. Elemental analysis, thermogravimetry and specific surface area:

The SSA of each silicate source was obtained via the B.E.T method using nitrogen adsorption on a TriStar surface area and porosity analyzer (Micrometrics) at CSIRO – Mineral Resources. The B.E.T specific surface area for the kaolinite and halloysite were determined to be $15.50 \pm 0.05 \text{ m}^2\text{g}^{-1}$ and $50.96 \pm 0.16 \text{ m}^2\text{g}^{-1}$ respectively. The elemental composition of each clay was determined by first mixing a sample of the clay (~0.25 g) with approximately 2 g of lithium borate in a Pt crucible and digested at 1000 °C for at least 30 minutes. The melt was then dissolved in 5% HNO₃ solution and brought to a known volume before the inductively coupled plasma – optical emission spectroscopy (ICP-OES) analysis, performed at CSIRO.

ICP-OES was also used to analyze the composition of the liquor samples obtained during each experiment. An aliquot of the resultant liquor after removal of any solids was diluted 100x in 2.5 % nitric acid (HNO₃) to stabilize the samples and then analyzed for Al, S, Na and Si concentrations using ICP-OES with an analysis error of less than 5.0 % ~~in each analysis~~. The average experimental error was calculated from duplicate experiments and includes evaporation, sampling and ICP analysis; this error was (with a 95% confidence) found to be $\pm 15.25\%$, where the samples at later times were more affected by evaporation, concentrating the liquor and increasing the error.

The thermogravimetric analysis (TGA) utilised a TA Instruments SDT Q600 simultaneous DTA-TGA. Approximately 20 mg of sample was weighed into a 110 μL platinum crucible with a matched empty crucible as a reference. The sample was heated from ambient to 800°C at 10°C per minute in an air atmosphere flowing at 100 ml per minute. The temperature scale of the instrument was calibrated using the melting points of 99.999% indium (156.5985°C), 99.99+% tin (231.93°C), 99.99+% zinc (419.53°C), and 99.99% silver (961.78°C). The balance was calibrated over the temperature range with alumina mass standards provided by the manufacturer. The heat flow between the pans was calibrated using a sapphire disk provided by the manufacturer. The cell constant was fine-tuned using the heat of fusion of zinc (113 J/g).

2.2.3. Vibrational spectroscopy:

Attenuated total reflection Fourier transform infrared (ATR-FTIR) spectra were obtained on a Nicolet-iS50 Spectrometer (Thermo Scientific) with a diamond ATR, 4 cm^{-1} resolution and 64 scans in total. This was used to evaluate the differences in the vibrational modes of the DSP phases formed at different times.

FTIR is a useful technique to differentiate the characteristic vibrational bands of the clay structures and the DSP formed. However, it is difficult to distinguish between the different phases of DSP formed (Barnes et al., 1999). Table 3 shows the characteristic bands found for SOD in the literature.

Table 3: Peaks observed in the IR spectrum for sodalite (where T is Si or Al).

Authors	Asymmetric stretch (Si – O – T)	Symmetric stretch	4- or 6- membered rings	T – O bend
Hermeler et al., 1991	986; 1086	660; 701; 729		
Adeeva and Vorsina, 1969	1000	660; 680; 710	565; 630	440
Barnes et al., 1999	980	734; 712; 660- 665	630-635	460

2.3.Desilication Test

Desilication tests were performed using a 2.0 L stainless steel vessel with agitation provided by an overhead stirrer (230 rpm) to ensure that the system is well mixed. The temperature of the liquor inside the vessel was controlled by a water bath and maintained constant during the experiment (90 °C). The vessel was sealed to reduce water evaporation and the ingress of atmospheric CO₂ into the liquor.

The desilication test was initiated once the temperature was achieved by adding the silicate source (at the initial reactive silica concentrations of low or high) to the liquor. Slurry samples were removed periodically at 5, 10, 15, 20, 30, 60, 120 and 180 minutes, placed in a centrifuge tube, sealed, allowed to cool and centrifuged for 4 minutes at 7000 rpm to separate the solids from the liquor. The sample volume chosen was to obtain a good quantity of solids for analysis, however, a small evaporation effect was observed at longer times which resulted in a slightly more concentrated liquor. Smaller aliquot volumes were also investigated and no difference in desilication behavior was observed.

The supernatant liquor was then collected for ICP analysis while the solids were washed with 100 ml DI water and collected by filtration (vacuum) using 0.2 µm filter paper (Supor Gelman membrane). The solids were dried overnight in an oven at 70 °C to avoid any possible phase transformation due to high temperatures.

3. Results and discussion

3.1.Characterization of starting solids

The starting materials were characterized to confirm their mineralogy. XRD patterns are shown in Figure 3 for the starting materials, halloysite and kaolinite. The database peaks for kaolinite (PDF# 00-058-200) are also shown for comparison. As would be expected, many of the peaks seen in the kaolinite pattern are also present in the halloysite pattern due the similarity in chemical composition and structure to kaolinite but broadened due to the shorter-range order present in halloysite.

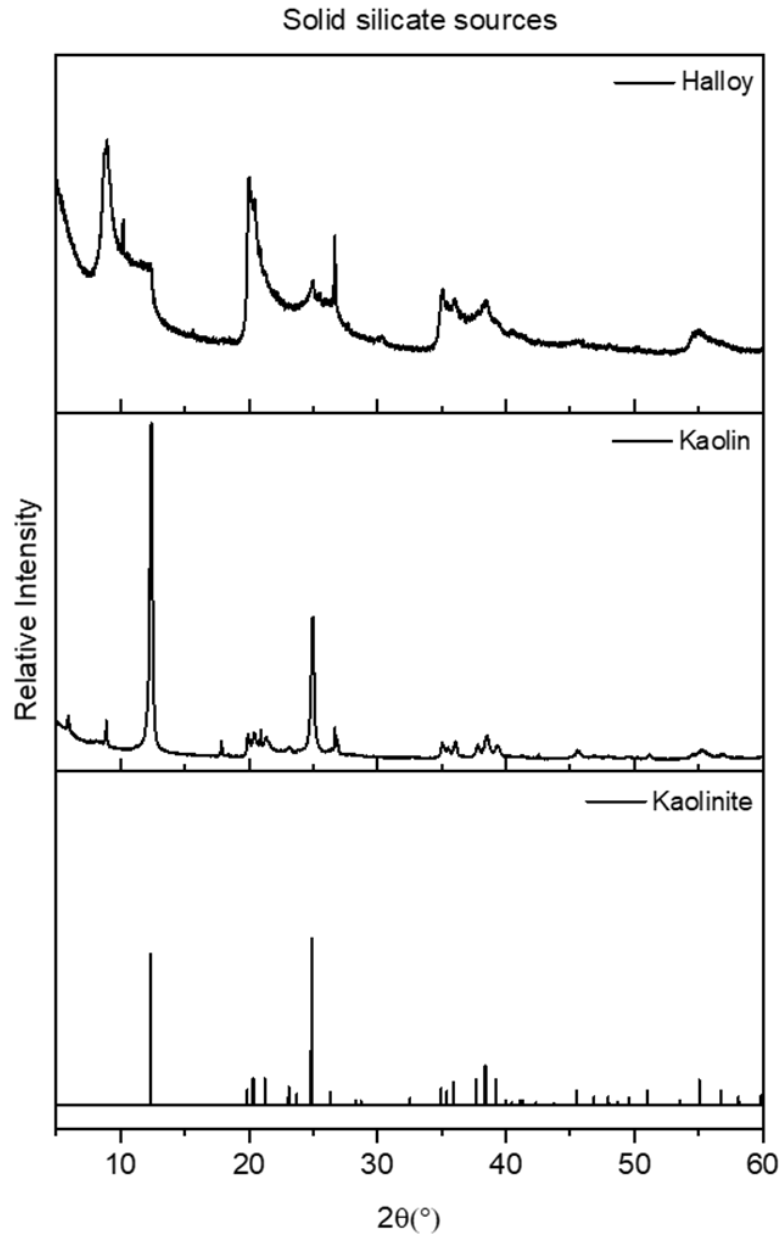


Figure 3: XRD patterns of the original kaolinite and halloysite samples used in experiments

The initial kaolinite morphology is shown in Figure 4a showing the major presence of platy kaolinite particles. Halloysite, by contrast, was identified by its tubular shape as can be seen in Figure 4b.

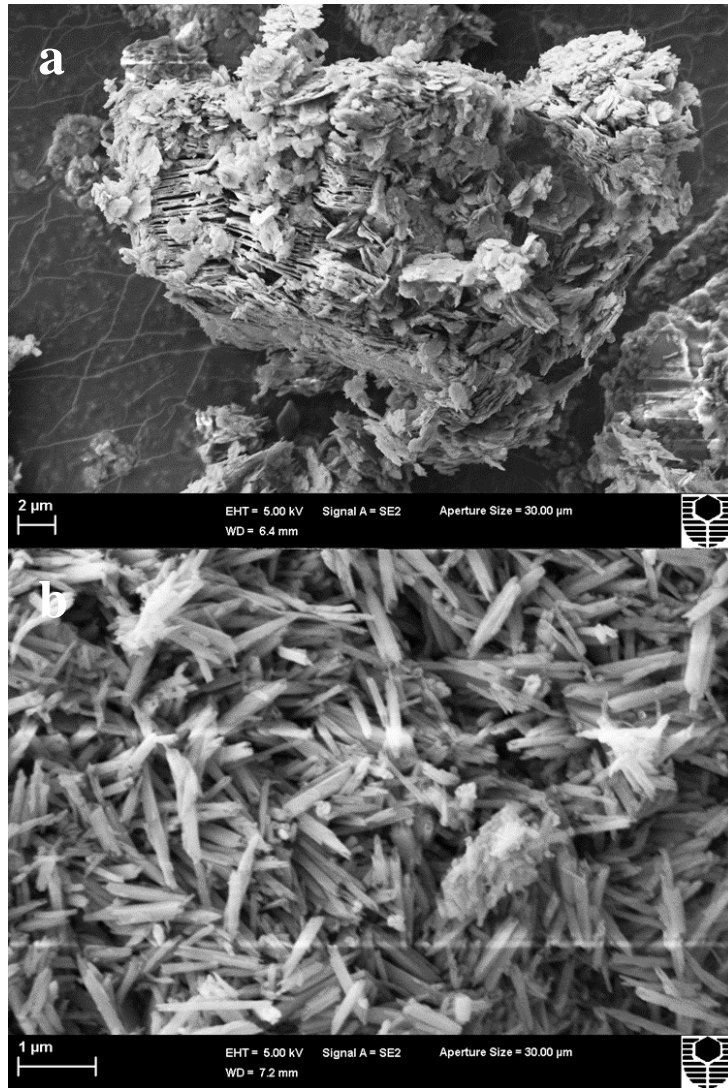


Figure 4: SEM image of the morphology of the original (a) kaolinite and (b) halloysite particles

The TGA curve (Figure 5) displays the weight (%) lost by the dehydration and dehydroxylation of the clays due to heating of the samples, up to 800 °C. Most of the removal of adsorbed and interstitial water present in the clay structures occurs up to 300 °C, with only minor water loss occurring between 300-400 °C (higher temperatures were not considered due to proximity to the phase transformation temperature), the structural transition and dehydroxylation of both clays occurs between 450 °C and 600 °C to give the amorphous meta- phase of the clays (Foldvari, 2011).

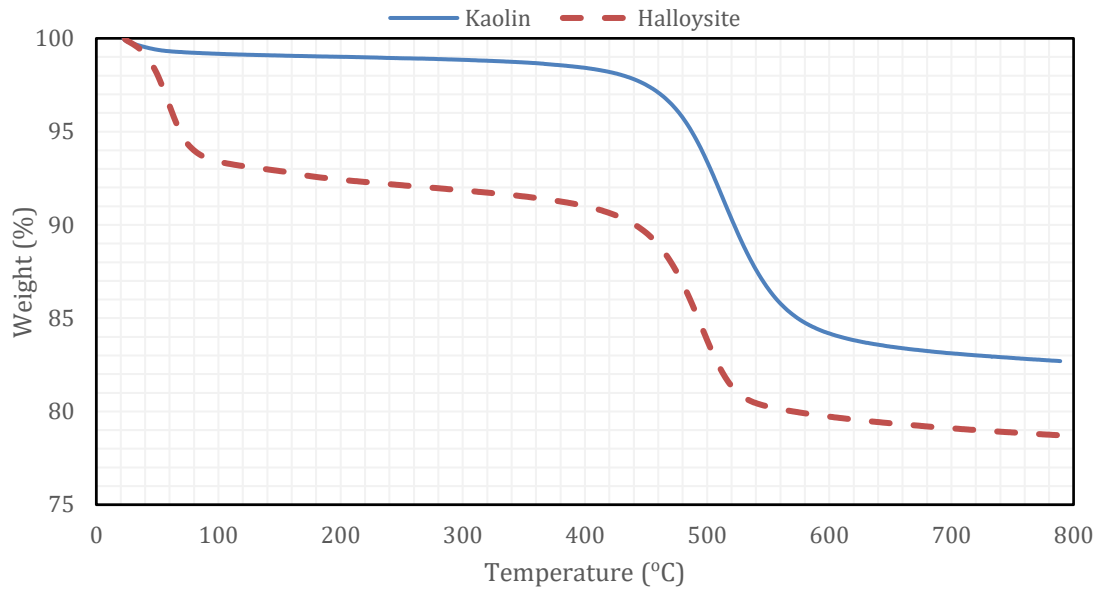


Figure 5: Weight (%) versus temperature (°C) of the original clay samples as determined from TGA

The TGA curve for halloysite, in contrast to that of kaolinite, indicates a higher bound water content shown by the initial weight loss up to 100 °C. The water content in the samples were calculated to be approximately 8.20 wt% for halloysite and 1.20 wt% for kaolinite. The elemental composition for both clays can be found in Table 3. The K₂O content suggests possible traces of muscovite present in the clay samples, particularly the kaolinite sample.

Table 4: Elemental composition, expressed in terms of their %oxides, of the kaolinite and halloysite clays used in experiments.

Chemical Composition (% Oxides)									
	Al ₂ O ₃	K ₂ O	Na ₂ O	SiO ₂	Fe ₂ O ₃	TiO ₂	CaO	MgO	Water
Kaolinite	28.54	0.39	0.13	51.26	1.51	0.32	0.04	N/A	1.20
Halloysite	33.48	0.10	0.04	42.46	0.41	0.02	0.09	0.03	8.20

Figure 6 shows the ATR-FTIR vibrational spectra of the untreated clay samples used in the experiments.

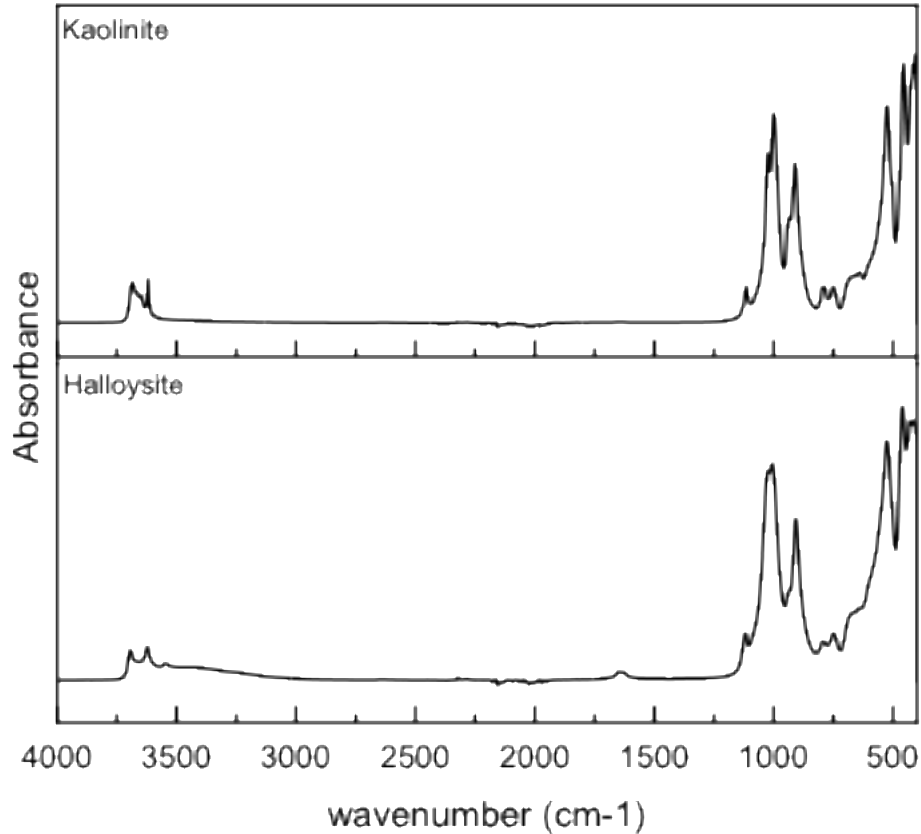


Figure 6: ATR-FTIR spectra of original clay samples used in experiments.

The similarity in the infrared spectra is to be expected on the basis of the similarity in structure of the two clays. Both spectra show the expected sharp bands in the OH stretching region ($3500 - 4000 \text{ cm}^{-1}$) representing the $\text{Al}(\text{OH})_2$ groups (N'Guessan et al., 2021) and the framework stretching bands in the $900\text{--}1000 \text{ cm}^{-1}$ region (N'Guessan et al., 2021).

3.2. 100% kaolinite

The kinetic curve of desilication in the presence of these impurities (Figure 7) shows a characteristic shape as previously observed by Smith *et al.* (2002).

In the control case (100% kaolinite) (Figure 7), the observed maximum solution $[\text{SiO}_2]$ in the liquor was reached at 30 and 60 minutes for the high and low RxSiO_2 charges, respectively. After this point, the rate of precipitation of DSP is greater than the dissolution rate, approaching the equilibrium $[\text{SiO}_2]$. Interestingly, the maximum observed concentration of 1.85 gL^{-1} is the same in both control cases, however, Breuer (1963) and Laws (2005) found that at a lower RxSiO_2 charge, a lower maximum solution $[\text{SiO}_2]$ in the liquor should be observed. The measured solution $[\text{SiO}_2]$ is a combination of the dissolution curve of the clay (shown as the dashed line in Figure 7 for the low RxSiO_2 case) and the precipitation curve of the DSP (shown as the dotted line in Figure 7 for the low RxSiO_2 case). The precipitation of the DSP begins prior to the measured maximum and ultimately precipitation dominates until a steady state silica concentration is reached. Thus, the complexity of the processes occurring and the time at which sampling occurred may mask small differences in the observed maximum

solution $[\text{SiO}_2]$ which may explain the same observed maxima for these different RxSiO_2 cases.

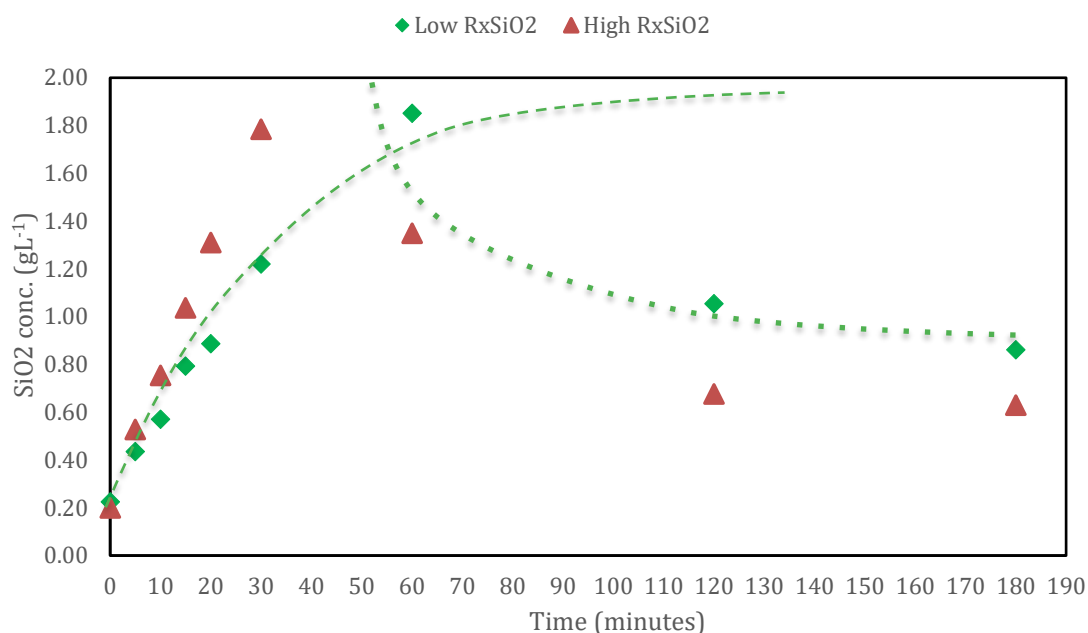


Figure 7: Solution $[\text{SiO}_2]$ versus time curves for low and high reactive silica levels for 100% kaolinite samples. Green dashed line qualitatively shows the dissolution and dotted line qualitatively describes DSP precipitation

The XRD patterns show the formation of the DSP with the peaks for the residual clays reducing with time (see *Supporting Information A*). The main DSP structure appearing in the XRD patterns was characteristic of sodalite (Nosean-PDF# 01-072-1614) with no other phases (including zeolite A) observed.

3.3. Varying halloysite: Low silicate levels

Initially, the effects of halloysite at 50% kaolinite and 50% halloysite of the total clay mass (low RxSiO_2) was observed and compared with the kaolinite only (also low RxSiO_2) situation in order to ascertain what effect the presence of a higher SSA and a more reactive clay would have on the kinetics of dissolution and the precipitation mechanism of DSP.

The clay dissolution kinetics in the presence of 50% halloysite was faster than 100% kaolinite (up to 30 min). In fact, for the 50% halloysite the solution $[\text{SiO}_2]$ in the liquor in the first 5 minutes was double compared to kaolinite only (Figure 8). This is probably an effect of a higher SSA on the dissolution of the clay. However, the precipitation of DSP or the difference between the dissolution of the clay species and the precipitation of DSPs appears to be slower after it has reached the maximum solution $[\text{SiO}_2]$ level in the liquor. The maximum solution $[\text{SiO}_2]$ measured for 100% kaolinite was 1.85 gL^{-1} at 60 min but when 50:50 kaolinite:halloysite was present the maximum was found to be 1.60 gL^{-1} at 30 min. Thus, while the maximum solution $[\text{SiO}_2]$ is similar, the peak occurs at different times. As stated previously, the maximum solution $[\text{SiO}_2]$ is a complex balance between the dissolution and re-precipitation reactions. In this case the 50% halloysite clay is dissolving faster but reaches a slightly lower observed maximum.

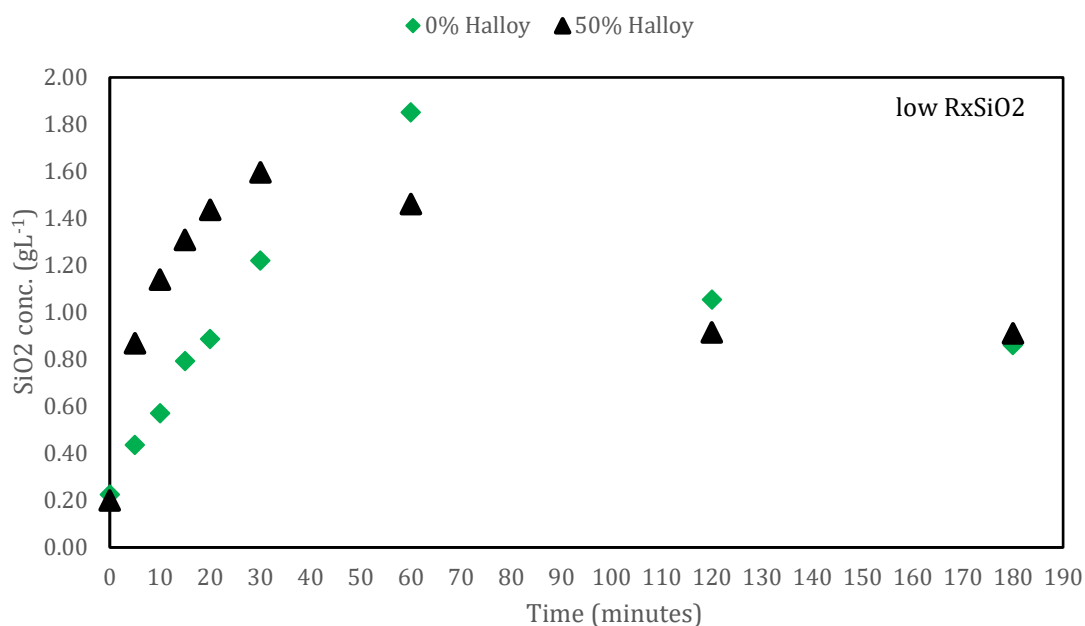


Figure 8: Solution $[\text{SiO}_2]$ versus time curves for low reactive silica charge having 100% kaolinite (0% halloysite) and 50:50 kaolinite:halloysite

Clearly, the effect of 50% of the RxSiO_2 being from a higher specific surface area and more reactive clay, in this case halloysite, results in faster dissolution of SiO_2 from the clay to the liquor but possibly a slower formation of DSP. The XRD (Figure 9) shows the appearance of sodalite peaks (110) and (211) at an earlier time (30 min) for the 50% halloysite sample compared to the 100% kaolinite (60 min). These times also correspond to the maximum solution $[\text{SiO}_2]$ in the liquor for both experiments (Figure 8). This suggests that the nucleation of the DSP started some time before the observed maximum solution $[\text{SiO}_2]$ in the liquor. From the XRD data we can observe higher kaolinite peaks ($25^\circ 2\theta$ for example) for the sample with halloysite at 120 min compared to the kaolinite only, this suggesting that the majority of the SiO_2 in the liquor is from halloysite. Thus, most of the kaolinite in this mixture is dissolving slowly and this may explain the subsequent slower decrease of solution $[\text{SiO}_2]$ when compared to 100% kaolinite. From this data, it appears (from the relative peak heights) that more SOD is formed and at earlier time (30min) when halloysite is present but once the halloysite has dissolved, dissolution and re-precipitation of the silica from the clay mixture at the low RxSiO_2 level is slower than the 100% kaolinite sample.

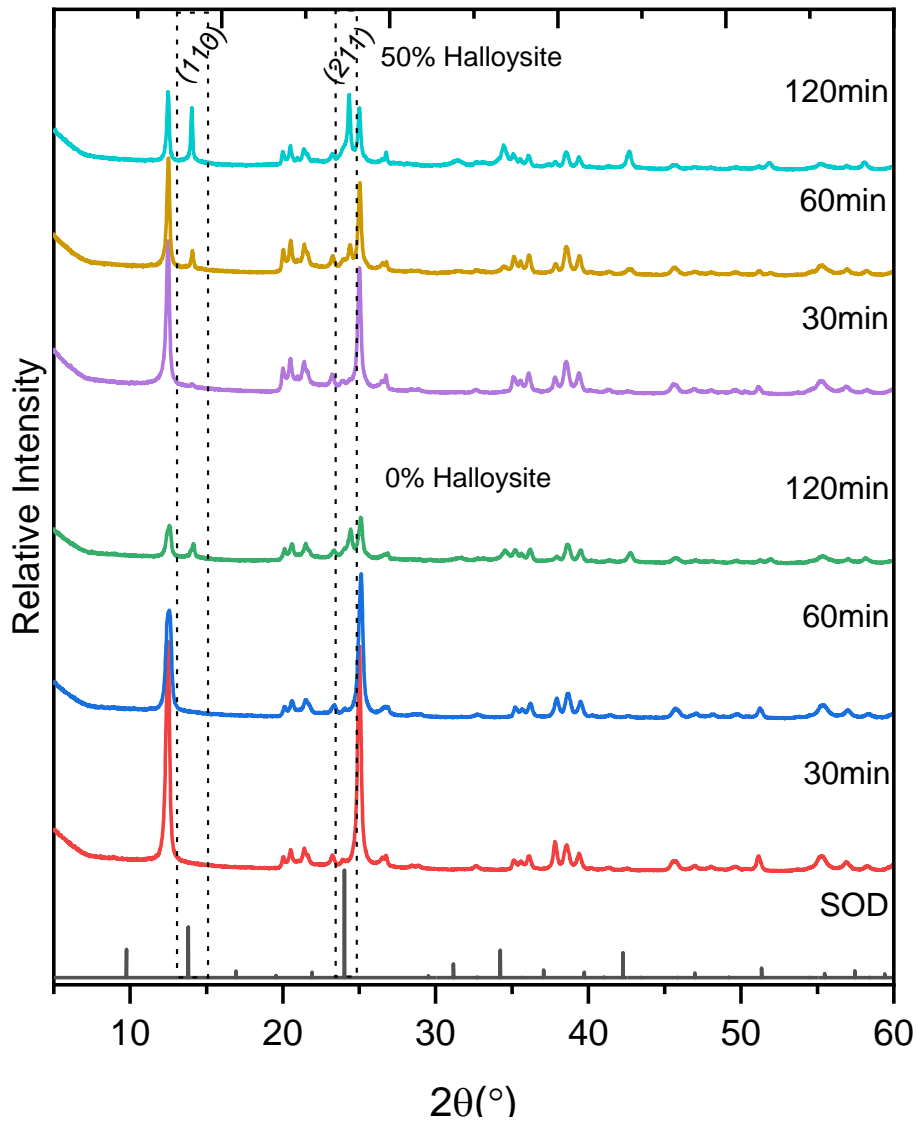


Figure 9: XRD patterns of solids collected at different times for 0% and 50% halloysite runs showing the earlier appearance of sodalite peaks (110) and (211), when halloysite is present (50%), compared to 0% halloysite.

3.4. Varying halloysite: High silicate levels

Figure 10 below illustrates how the presence of increasing halloysite results in increases in the observed maximum solution $[\text{SiO}_2]$ in the liquor and these maxima occur at shorter times as the content of halloysite increases. Unlike at the lower RxSiO_2 case where the 50% halloysite showed a slower DSP precipitation rate of $[\text{SiO}_2]$ decrease after the maximum is reached, at the higher RxSiO_2 increased precipitation rates are observed. Thus, not only is the dissolution faster, reaching a higher observed maximum solution $[\text{SiO}_2]$, but the solution $[\text{SiO}_2]$ in the liquor drops more rapidly when more halloysite is present. The drop in solution $[\text{SiO}_2]$ is due to DSP formation, that is by the precipitation of new phases confirmed through XRD and FTIR.

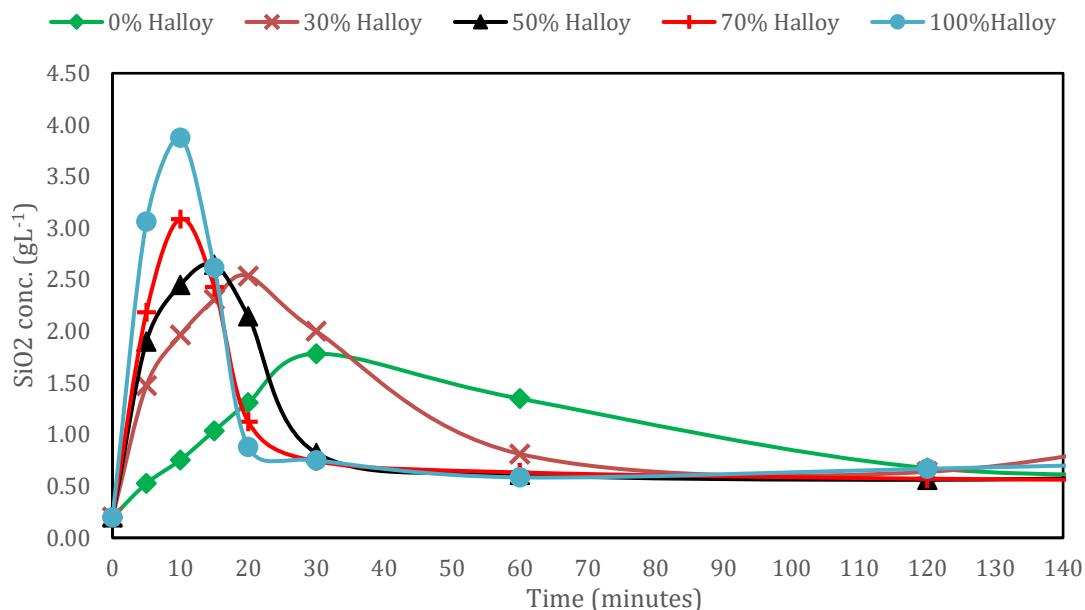


Figure 10: Solution $[\text{SiO}_2]$ versus time curves for varying halloysite content (lines to guide reader only)

As the halloysite content increases the observed maximum solution $[\text{SiO}_2]$ increases from 2.54 gL^{-1} , 2.65 gL^{-1} , 3.09 gL^{-1} and 3.88 gL^{-1} for 30%, 50%, 70% and 100% halloysite, respectively, with the main change occurring in the first 5 min. This increased dissolved silicate level occurs at shorter and shorter times and would result in a higher driving force for the precipitation of DSP solids and reduces the time at which the DSP phases are observed. The DSP phases formed during the desilication of the liquor in the different cases are shown in the XRD patterns (see *Supporting Information A*). Qualitative information on how much clay and DSP was present at each of the sample times was determined from analysis of the XRD patterns (see *Supporting Information A1*). This showed that in the presence of 100% halloysite almost all of the clay (80-100%) had dissolved by the 120 minute mark while ~60% of the kaolinite was still present at 120 minutes in the 100% kaolinite experiment.

4. Discussion

The kaolinite only results (Figure 7) show an unexpected result in similar observed maximum solution $[\text{SiO}_2]$ despite the differences in total SSA between the low and high R_xSiO_2 cases. When 50:50 kaolinite:halloysite is compared to 100% kaolinite (Figure 8) it is observed that 100% kaolinite reaches a higher solution $[\text{SiO}_2]$ in the liquor before the onset of DSP precipitation compared to 50% halloysite. At this higher supersaturation level more DSP nuclei *should* be produced, which then *should* result in a faster DSP precipitation. While the 50% halloysite case results in quicker dissolution a slower decline in solution $[\text{SiO}_2]$ during the DSP precipitation stage is observed. One possible explanation for this behaviour is that a lower supersaturation is required for DSP to form in the 50% halloysite case. This would result in fewer DSP nuclei precipitation and therefore could result in a slower DSP formation rate. The question is why does halloysite require a lower dissolved silicate concentration for DSP formation despite faster dissolution? For both the pure kaolinite and the 50:50 sample the difference in the observed maximum liquor silica concentration is only small, 1.6 vs

1.8 gL⁻¹, thus this *may* mean the difference in the desilication rate is within error (especially when sampling times are also considered).

At high RxSiO₂ (Figure 10) the increasing % of halloysite present is clearly linked to both an increase in the maximum solution [SiO₂] and an increase in the subsequent rate of DSP formation. The ~~morphology of the~~ untreated halloysite tubes, due to the presence of water in the interlayers (10 Å), causes a lateral mismatch of the tetrahedral and octahedral sheets (Paskakhsh et al., 2013). In the first 5 minutes of the experiment, a dehydration effect of the halloysite tubes can be observed as the basal spacing changes from 10 Å to 7 Å (Figure 11), modifying the initial structure of the halloysite tubes (Joussein, 2016). From the XRD patterns of the solid products from experiments with 30% and 50% halloysite (see *Supporting Information A*) a peak characteristic of SOD appears at 30 min. With 70% and 100% halloysite, the DSP peak characteristic of SOD appears much earlier at around 15 min, confirming the behaviour observed in Figure 10. The observation of the SOD peaks in the XRD occur right after the [SiO₂] ~~concentration~~ in the liquor has dropped from the maximum solution [SiO₂]. This increase in DSP precipitation can be understood in terms of the ~~which is due to the~~ greater driving force present when the solution [SiO₂] is higher ~~for the precipitation of DSP~~.

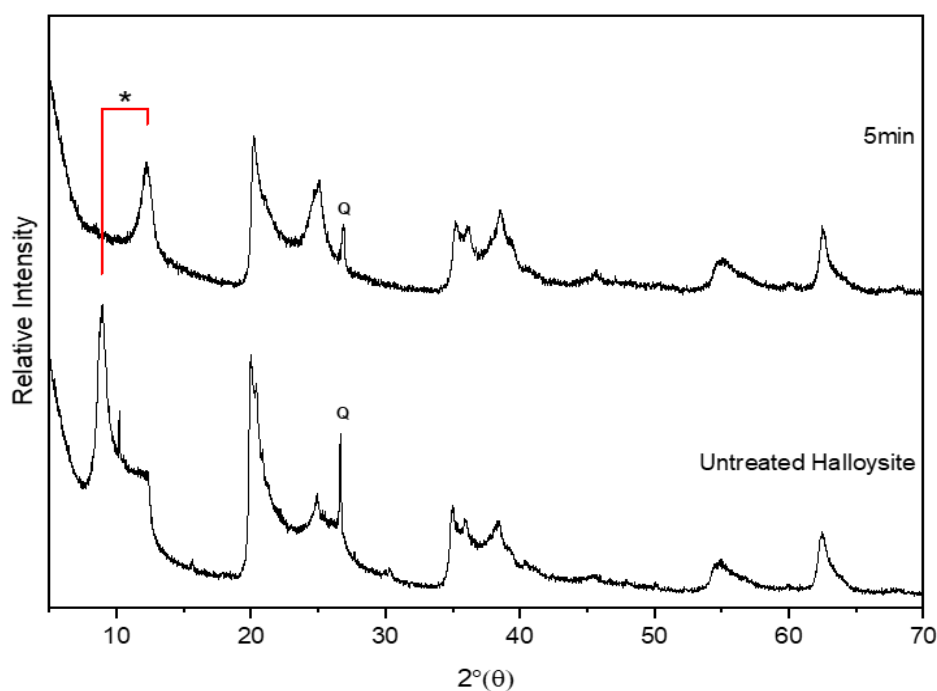


Figure 11: XRD patterns of untreated halloysite and after 5 min in Bayer liquor, showing the dehydration effect (*) on the structure of the halloysite nanotubes (Q – unreactive Quartz peak)

The FTIR spectra (and the corresponding vibrational bands) of the untreated clay samples and the DSP formed in synthetic Bayer liquor at different times for the 0%, 50% and 100% halloysite samples are shown in the *Supporting Information B*. The major changes observed in the vibrational spectra are attributed to the overall decrease in the intensity of the –OH stretching vibration in the range of 3700 to 3600 cm⁻¹ due to the clays dissolving and the formation of the strongest absorption band at 970 to 980 cm⁻¹, which is consistent with the literature value for SOD (Table 3) ~~and is associated~~

to the asymmetric stretching of the SOD framework Al—O—Si. This band is seen to be formed at 60 min and 180 min.

To investigate the mechanism of the clay dissolution and the DSP formation, morphological SEM images were also taken of the samples obtained at different times in an attempt to observe any unusual effect caused by the presence of halloysite tubes on the DSP precipitation. It is possible to observe from the SEM images of the solids collected at 30 min for the 100% halloysite and 100% kaolinite (50:50 ratio) sample that SOD forms at the edges of the platy kaolinite layers (Figure 12) and at the ends of the halloysite tubes (Figure 13). This is in agreement with (Radomirovic et al., 2013), confirming the initial heterogeneous nucleation of the SOD particles on kaolinite edges.

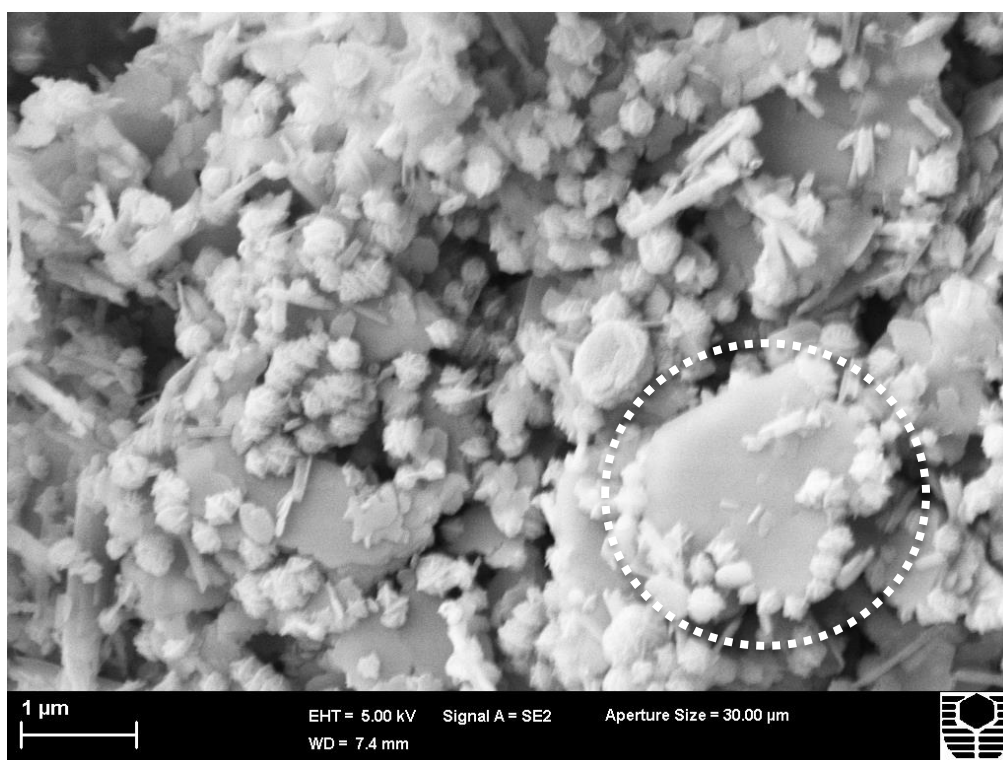


Figure 12: SEM of the solids collected at 30 min for case 2 (100% kaolinite) – sodalite particles can be seen at the edges of the clay particles

In the case of halloysite, White *et al.* (2012) observed that the dissolution of the tubes initiated from the inner surfaces and the exposed Al – OH groups. These are highly reactive, causing a progressive thinning of the tubes from the inside-out. This is in agreement with our results as the presence of thinner and collapsed tubes were present in the SEM (Figure 14) and TEM images (see *Supporting Information Figure C1*).

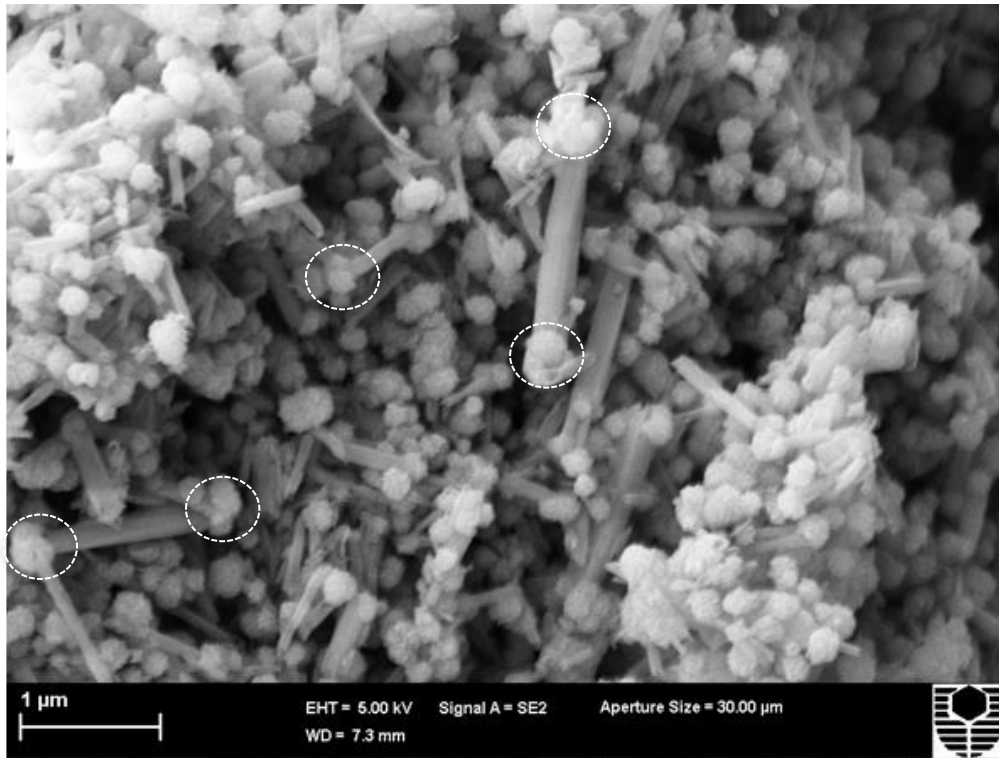


Figure 13: SEM of the solids collected at 30 min for case 4 (100%halloysite) – sodalite particles can be seen at the ends of tubular halloysite

This suggests that the reaction between exposed Al – OH and Si – OH groups located on the edges and on defects of the clay minerals with the free caustic in synthetic Bayer liquor prompts the dissolution of the clay and subsequent formation of SOD ~~without an intermediate phase in the presence of Na_2CO_3 (20 gL^{-1}) and Na_2SO_4 (15 gL^{-1})~~. Thus, in the case of kaolinite, sodalite particles grow on the edges of the layers and on defects while the basal surface is relatively inert (see *Supporting Information Figure D2*).

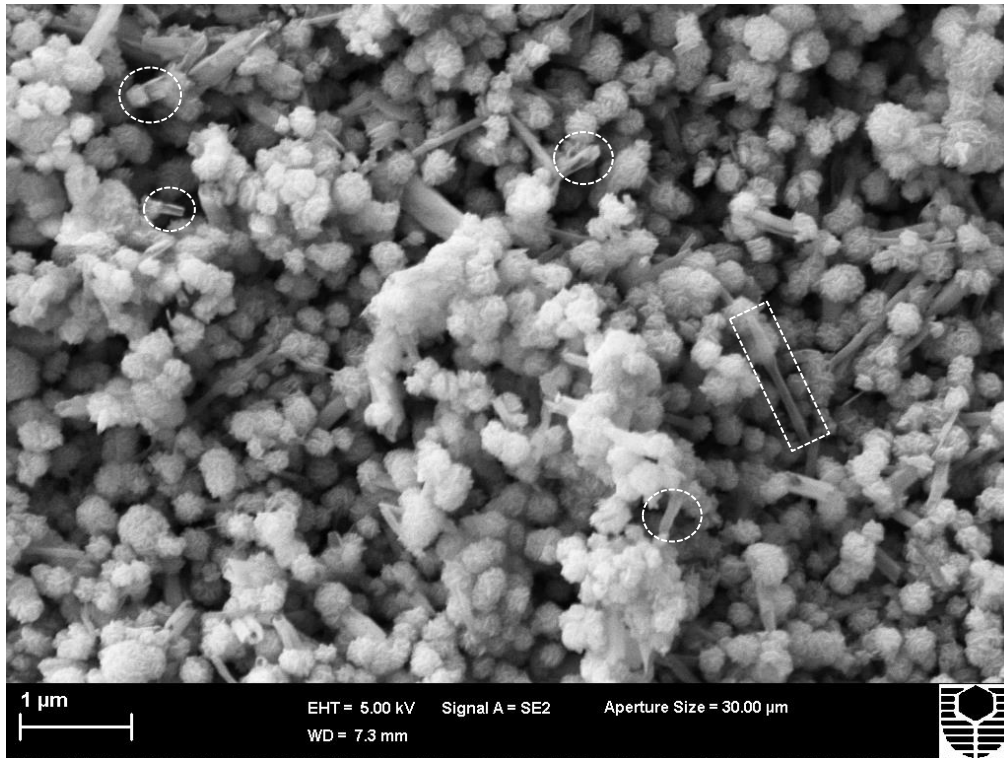


Figure 14: SEM image of solids collected from case 4 (100% halloysite) after 120 minutes showing the presence of collapsed and thinner halloysite tubes

TEM analysis of the solids at 60 min confirmed much of the information already obtained (Figure 15). The halloysite at this time had a (thickness of ~ 85.0 nm) but the samples were beam sensitive, due to dehydration, and deformed over time (see *Supporting Information Figure C4*). The SOD was seen to be present as essentially spherical particles. EDS mapping showed that sulfur was present in the DSP but not in the halloysite as expected.

The fitting of the XRD patterns showed that the dissolution of halloysite is indeed significantly faster than that of kaolinite, with $>80\%$ of the halloysite dissolved by 120 minutes while only $\sim 40\%$ of kaolinite is dissolved by this time (*Supporting Information A1*).

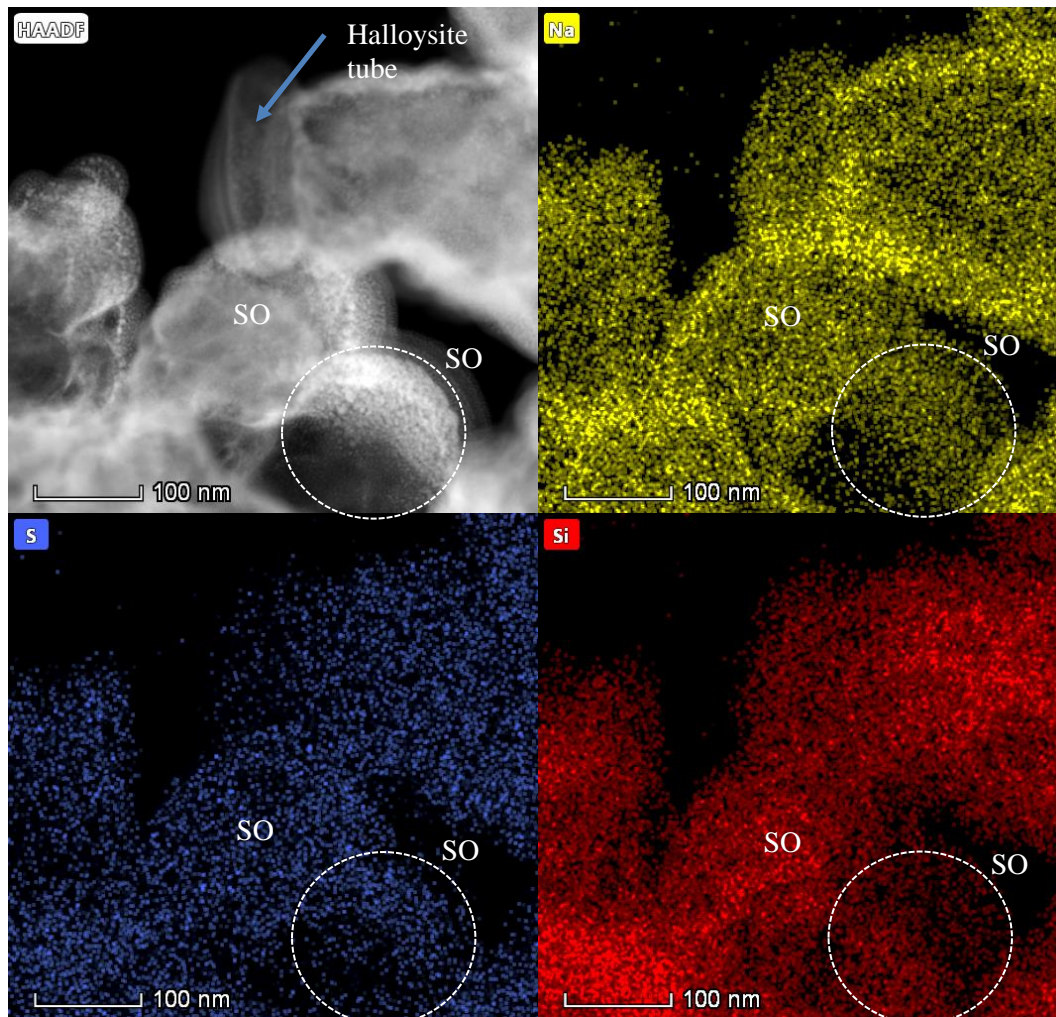


Figure 15: TEM images of DSPs obtained from case 4 (100% haloysite) at 60 min and the respective EDS mapping of Na, S and Si, showing the presence of S in the SOD structure

The LTA phase has been previously observed in experiments using soluble metasilicate but is absent when sulfate ions are present (Peng et al., 2018). Similarly, an amorphous phase has been observed with soluble metasilicate (Radomirovic et al., 2013) but no significant amorphous phase was observed in any of these reactions. Similarly, no discernable LTA phase was observed either in the presence of haloysite or kaolinite or any of the different mixtures thereof. The absence of zeolite LTA peaks may be due to a templating effect of the solid silicate source (kaolinite and haloysite), the presence of sulphate ions in the liquor (Peng et al., 2018) or may be a detection limit issue.

4.1 Analysis and determination of total surface area impact

Roach and White (1998) had previously observed some of the effects caused by the presence of the more reactive haloysite in their bauxite samples, however, no quantification of the ratios of ~~pure kaolin~~ (kaolinite) and haloysite was attempted. In this work, the haloysite content is controlled and known so it is possible to further investigate how the different ratios of haloysite affected the kinetics (Figure 10) of dissolution. Thus, by interrogating the data in the dissolution phase of the reaction it can be assessed whether there is a correlation with the higher reactivity of the haloysite

and/or the higher total SSA of the clay composition (see Table 1, Table 5 and further discussions below).

The increased ratio of halloysite in the different cases not only increased the maximum solution $[\text{SiO}_2]$ values but also decreased the time for the maximum value to be reached. In the 0% halloysite case, the maximum was reached at 30 min with approximately $1.78 \text{ gL}^{-1} [\text{SiO}_2]$ dissolved.

Table 5: The maximum solution $[\text{SiO}_2]$ and time maximum was observed for each experiment.

Halloysite (wt%)	Maximum solution $[\text{SiO}_2]$ (gL^{-1})	t_{maximum} (min)	Total SSA BET (m^2)
0	1.78	30	340.80
30	2.54	20	574.90
50	2.65	15	731.00
70	3.09	10	887.00
100	3.88	10	1121.10

~~With the focus on the effects caused by the changes of the total SSA of the clay samples by adding different amounts of halloysite at relatively constant R_xSiO_2 levels, the kinetics of dissolution were assessed. The real question is, however, whether halloysite behaves differently to kaolinite in the highly alkaline liquor? Firstly, it was ascertained whether the change in dissolution rate could be explained by the increased surface area present.~~

Using the data in Table 5 the impact of the increased total specific surface area on the dissolution of the clays, can be estimated by taking the slope to the maximum solution $[\text{SiO}_2]$ peak in the liquor. This was done and the relationship to increased SSA was determined (Figure 16). Clearly, there is a relationship between dissolution rate and the initial total SSA of the solid mixture. Gautier *et al.*, (2001) and Okau and Yamada (2013) studied the dissolution of quartz to understand the effects of surface area during the dissolution process. While Gautier *et al.*, (2001) found geometric surface area to be a better parameter for describing the impact on dissolution kinetics of quartz Oku and Yamada (2013) found the SSA to be the better descriptor. The results shown in Figure 16 are in agreement with ~~the results shown by Oku and Yamada, (2013) in which the rate of dissolution increased with the surface area of quartz.~~ This result suggests that the dissolution kinetics follow a first order relationship with total SSA and there is nothing exceptional about the halloysite dissolution behaviour. That is, the surface area change is sufficient to explain the change in dissolution rate and the crystallinity of the halloysite does not significantly impact the kinetics.

Effect of Surface Area - High RxSiO₂

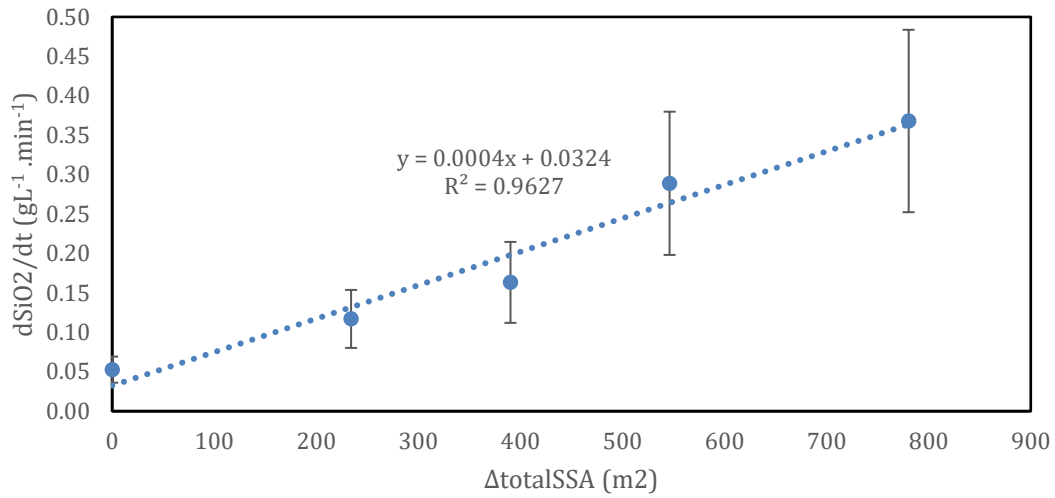


Figure 16: The rate of dissolution versus Δ Total SSA, showing a linear relationship

Thus, based on the Oku and Yamada (2013) relationship:

$$\frac{d[\text{SiO}_2]}{dt} = kS[\text{OH}^-]^n \quad \text{Equation 1}$$

where k is the rate constant, S is the total SSA of the solids and n is the order with respect to hydroxide concentration. Therefore, the initial dissolution of the RxSiO₂ into the liquor is dependent on the initial total SSA of the clay samples. This suggests that halloysite and kaolinite behave similarly chemically but it is the physical difference in surface area that is impacting the dissolution rate.

The increase in the solution [SiO₂] from the dissolution of the clay samples to the liquor also impacts the number of nuclei formed as the nucleation of particles will depend on the supersaturation. Once nucleation occurs, growth and other processes (such as secondary nucleation) can take place. Beyond the maximum, the decrease in silica concentration should show the following relationship (Jones and Smith, 2008):

$$-\frac{d[\text{SiO}_2]}{dt} = k'A_{dsp}(SR - 1)^m \quad \text{Equation 2}$$

where A_{dsp} is the DSP surface area and SR is the silica supersaturation ratio ($[\text{SiO}_2]_i/[\text{SiO}_2]_{eq}$). The SSA plays a significant role on the rate of dissolution of the clay and consequently on the formation of the DSPs. Therefore, changes caused by an increase of the total SSA (or any other area directly related to the total SSA) due to the presence of halloysite in the bauxite will impact the formation kinetics of the DSPs.

5. Conclusions

In this report, known ratios of kaolinite and halloysite were investigated to determine the effects on the kinetics of dissolution and the precipitation pathway of the DSP phase (SOD).

The effect of an increased SSA, caused by the presence of different ratios of halloysite clay, leads to faster dissolution of the $RxSiO_2$ into the liquor. The presence of halloysite also increases the observed maximum solution $[SiO_2]$ value in the liquor even when the total amount of $RxSiO_2$ is constant. ~~The higher maximum solution $[SiO_2]$ in the liquor contributes to a greater driving force to form DSP particles.~~ Higher solution $[SiO_2]$ result in greater driving force for DSP nucleation and this results in higher nuclei numbers and faster desilication kinetics of the liquor.

Kaolinite and the presence of halloysite did not show any evidence of an amorphous or LTA phase formed. However, is this due to the presence of sulphate in the Bayer liquor (Smith et al., 2002 ; Peng et al., 2018), limit of detection or is this a templating effect of the clay? Further work is required to answer this question. The sodalite formed was initially predominantly at edges and defects of the kaolinite and at the ends of the halloysite tubes. This suggests that the initial mechanism of formation is through heterogeneous nucleation.

The relationship between dissolution rate and total SSA is linear suggesting only minor impact of the halloysite crystallinity on dissolution kinetics. In addition, higher maximum solution $[SiO_2]$ are achieved when halloysite is present. At this stage most bauxite characterization does not differentiate between kaolinite and halloysite. However, this study suggests that the presence of halloysite with higher SSA, ~~behaves differently to kaolinite kinetically and so~~ if present, could affect the pre-desilication stage due to faster dissolution and also to higher observed maximum solution $[SiO_2]$. The presence of a high content of halloysite in the $RxSiO_2$ is seen to reduce the time necessary to achieve supersaturation, eventual DSP formation and equilibrium $[SiO_2]$ levels. Halloysite has the potential to increase desilication kinetics and thus increase the pre-desilication and digestion efficiencies.

Acknowledgements

We would like to acknowledge the John de Laeter Centre, Curtin University for use of the electron microscope facility and XRD instrument (ARC LE130100053, LE140100150, LE0775551), in particular Dr. Matthew Rowles for his assistance with the direct derivation method, and CSIRO for access to some of their facilities. J. Gomez would also like to acknowledge the AQW (Alumina Quality Workshop) and Curtin University for an Australian postgraduate award.

References

Adeeva, T. I. and Vorsina, I. A., 1969. "IR spectra of low-silica sodium hydroaluminosilicates" *Non-ferrous metals*, **42**, 2051-2055.

Anand, R. R., Gilkes, R. J. and Roach, G. J. D., 1991. "Geochemical and mineralogical characteristics of bauxites, Darling Range, Western Australia" *Applied Geochemistry*, **6**(3), 233-248. [https://doi.org/10.1016/0883-2927\(91\)90001-6](https://doi.org/10.1016/0883-2927(91)90001-6)

Barnes, M. C., 1999. "*The kinetics and mechanisms of sodium aluminosilicate crystallization in Bayer process scale formation*" PhD Thesis: University of South Australia.

Barnes, M. C., Addai-Mensah, J. and Gerson, A. R., 1999. "A methodology for quantifying sodalite and cancrinite phase mixtures and the kinetics of the sodalite to cancrinite phase transformation" *Microporous and Mesoporous materials*, **31**, 303-319. [https://doi.org/10.1016/S1387-1811\(99\)00080-3](https://doi.org/10.1016/S1387-1811(99)00080-3)

Bauer, A., Velde, B. and Berger, G., 1998. "Kaolinite transformation in high molar KOH solutions" *Applied Geochemistry*, **13**, 619-629. [https://doi.org/10.1016/S0883-2927\(97\)00094-2](https://doi.org/10.1016/S0883-2927(97)00094-2)

Breuer, R., Barsotti, L. and Kelly, A., 1963. "Behaviour of silica in sodium aluminate solutions" *Metallurgy of Aluminium*, **1**, 133-157.

Cardile, C. M., Willing, M. J. and Hughes, C. A., 1994. "Conversion of kaolin to DSP in the Bayer process" in *Extractive Metallurgy*, Publisher: AusIMM, pp. 321-324. ISBN:0949106968.

Carroll-Webb, S. A. and Walther, J. V., 1988. "A surface complex reaction model for the pH-dependence of corundum and kaolinite dissolution rates" *Geochimica & Cosmochimica Acta*, **52**, 2609-2623. [https://doi.org/10.1016/0016-7037\(88\)90030-0](https://doi.org/10.1016/0016-7037(88)90030-0)

Connop, W., 1996. "A new procedure for the determination of alumina, caustic and carbonate in Bayer liquor" *Proceedings of the 4th International Alumina Quality workshop, Darwin, Australia, Vol 2*, 321-330.

N'Guessan, N. E., Joussein, E., Courtin-Nomade, A., Paineau, E., Soubrand, M., Grauby, O., Robin, V., Cristina, C. D., Vantelon, D., Launois, P., Fondanèche, P., Rossignol, S., Texier-Mandoki, N. and Bourbon, X. 2021 "Role of cations on the dissolution mechanism of kaolinite in high alkaline media" *Applied Clay Science*, **205**, 106037-106049. <https://doi.org/10.1016/j.clay.2021.106037>

Foldvari, M., 2011. *Handbook of thermogravimetric systems of minerals and its uses in geological practices* Editor: Gyula Maros, Publisher: Geological Institute of Hungary, Budapest, Vol 213, pages 69, 71.

Freyssinet, P., Butt, C., Morris, R. and Plantone, P., 2005. "Ore forming processes related to lateritic weathering" In: *Economic Geology - One Hundredth Anniversary*. Eds: Hedenquist, J. W., Thompson J. F. H., Goldfarb, R. J. and Richards, J. P. Publisher: Society of Economic Geologists, Inc. Littleton, Colorado, 681-722.

Gan, B. K., Taylor, Z., Xu, B., van Riessen, A., Hart, R. D., Wang, X. and Smith, P., 2013. "Quantitative phase analysis of bauxites and their dissolution products"

International Journal of Mineral Processing, **123**, 64-72.
<https://doi.org/10.1016/j.minpro.2013.05.005>

Gautier, J., Oelkers, E. and Schott, J., 2001. "Are quartz dissolution rates proportional to B.E.T. surface areas?" *Geochimica et Cosmochimica Acta.*, **65**, 1059-1070.
[https://doi.org/10.1016/S0016-7037\(00\)00570-6](https://doi.org/10.1016/S0016-7037(00)00570-6)

Hermeler, G., Buhl, J. and Hoffmann, W., 1991. "The influence of carbonate on the synthesis of an intermediate phase between sodalite and cancrinite" *Catalysis Today*, **8(4)**, 415-426. [https://doi.org/10.1016/0920-5861\(91\)87020-N](https://doi.org/10.1016/0920-5861(91)87020-N)

Hose, H., 2013. "Bauxite Mineralogy" in *Essential Readings in Light Metals: Alumina and Bauxite*, Editors: Donaldson, D. and Raahauge, B., Publisher: Wiley, Vol 1, 21-29.
<https://doi.org/10.1002/9781118647868.ch2>

Jones, F. and Smith, P., 2008. "What is the kinetic order of desilication?" Proceedings of the 8th International Alumina Quality Workshop. Darwin, N.T., 100-102.

Joussein, E., 2016. "Geology and mineralogy of nanosized tubular halloysite" In: *Nanosized Tubular Clay Minerals Vol 7: Halloysite and Imogolite*. Editors: Yuan, P., Thill, A., Bergaya, F., Publisher: Elsevier, 12-48.

LaMacchia, R., 2012. "Toward a better understanding of desilication product (DSP) precipitation kinetics" Proceedings of the 9th International Alumina Quality Workshop, Perth, Western Australia, 214-218.

Laws, M. P., 2005. "*Reaction of kaolinite in the pre-desilication processing of bauxite ores*" PhD Dissertation, University of Melbourne.

Oku, T. and Yamada, K., 2013. "The dissolution rate of quartz and the rate of desilication in the Bayer liquor" *Essential Readings in Light Metals: Alumina and Bauxite*, Editors: Donaldson, D. and Raahauge, B., Publisher: Wiley, Vol 1, pp. 247-254. <https://doi.org/10.1002/9781118647868.ch33>

Pasbakhsh, P., Churchman, G. J. and Keeling, J. L., 2013. "Characterisation of properties of various halloysites relevant to their use as nanotubes and microfillers" *Applied Clay Science*, **74**, 47-57. <https://doi.org/10.1016/j.clay.2012.06.014>

Peng, H., Ding, M. and Vaughan, J., 2018. "The anion effect on Zeolite Linde Type A to Sodalite phase transformation" *Industrial and Engineering Chemistry Research*, **57(31)**, 10292-10302. <https://doi.org/10.1021/acs.iecr.8b02026>

Radomirovic, T., Smith, P., Southam, D., Tashi, S. and Jones, F., 2013. "Crystallization of sodalite particles under Bayer-type conditions" *Hydrometallurgy*, **137**, 84-91.
<https://doi.org/10.1016/j.hydromet.2013.05.006>

Roach, G. I. D. and White, A. J., 1988. "Dissolution kinetics of kaolin in caustic liquors" Light Metals, 41-47 or b) year 2016 in *Essential Readings in Light Metals*, Editors: Donaldson, D. and Raahauge, B., Publisher: Springer, 240-246.
https://doi.org/10.1007/978-3-319-48176-0_32

Schott, J., Pokrovsky, O. S. and Oelkers, E. H., 2009. "The link between mineral dissolution/precipitation kinetics and solution chemistry" *Reviews in Mineralogy & Geochemistry*, **70**, 207-258. DOI: 10.2138/rmg.2009.70.6

Smith, P., 2009. "The processing of high silica bauxites - review of existing and potential processes" *Hydrometallurgy*, **98**, 162-176. <https://doi.org/10.1016/j.hydromet.2009.04.015>

Smith, P. G., Lowe, J. L., Rohl, A. L, Penniford, R. M. and Parkinson, G. M., 2002. "Understanding growth of DSP in the presence of inorganic ions" Proceedings of the 6th International Alumina Quality Workshop, Brisbane, Queensland, 191-194. <http://hdl.handle.net/102.100.100/199209?index=1>

Smith, P., Penniford, R., Lwin, T. and Kane, A., 2001. "The composition of DSP formed under pre-desilication and high temperature Bayer digestion conditions" *Light Metals*, New Orleans, LA, Minerals, Metals and Materials Society/AIME, 184 Thorn Hill Road, Warrendale, PA 15086-7528, USA.5-11.

Smith, P., Wingate, C. and De Silva, L., 2008. "Mobility of included soda in sodalite" Proceedings of the 8th International Alumina Quality Workshop. Darwin, N.T., 27-30.

Toraya, H. 2018 "Direct derivation (DD) of weight fractions of individual crystalline phases from observed intensities and chemical composition data: incorporation of the DD method into the whole-powder-pattern fitting procedure" *Journal of Applied Crystallography*, 51(2), 446-455 <https://doi.org/10.1107/S1600576718001474>

Tan, D., Yuan, P., Liu, D. and Du, P., 2016. "Surface modifications of halloysite" In: *Nanosized Tubular Clay Minerals Volø 7: Halloysite and Imogolite*. Editors: Yuan, P., Thill, A., Bergaya, F., Publisher: Elsevier, 167-201.

Vogrin, J., Vaughan, J., Peng, H. and Santini, T., 2018. "Characterization and steps toward structure solution of synthetic anion-substituted desilication products" Proceedings of the 12th International Alumina Quality Workshop. Gladstone, Queensland, 233-240.

White, R. D., Bavykin, D. and Walsh, F., 2012. "The stability of halloysite nanotubes in acidic and alkaline aqueous suspensions" *Nanotechnology*, **23** (6), 065705. DOI: 10.1088/0957-4484/23/6/065705

Yuan, P., Tan, D. and Bergaya, F. A., 2015. "Properties and applications of halloysite nanotubes: recent research advances and future prospects" *Applied Clay Science*, **112-113**, 75-93. <https://doi.org/10.1016/j.clay.2015.05.001>